Available online at www.sciencedirect.com
SCIENCE DIRECT®
Journal of Solid State Chemistry 179 (2006) 378–388
JOURNAL OF SOLID STATE CHEMISTRY
www.elsevier.com/locate/jssc

Mn^{4+} environment in layered $Li[Mg_{0.5-x}Ni_xMn_{0.5}]O_2$ oxides monitored by EPR spectroscopy

R. Stoyanova[a,*], E. Zhecheva[a], S. Vassilev[b]

[a]Institute of General and Inorganic Chemistry, Bulgarian Academy of Sciences, 1113 Sofia, Bulgaria
[b]Institute of Electrochemistry and Energy Systems, Bulgarian Academy of Sciences, 1113 Sofia, Bulgaria

Received 12 September 2005; received in revised form 19 October 2005; accepted 20 October 2005
Available online 1 December 2005

Abstract

X-band and high-frequency EPR spectroscopy were used for studying the manganese environment in layered $Li[Mg_xNi_{0.5-x}Mn_{0.5}]O_2$, $0 \leqslant x \leqslant 0.5$. Both layered $LiMg_{0.5}Mn_{0.5}O_2$ and monoclinic $Li[Li_{1/3}Mn_{2/3}]O_2$ oxides (containing Mn^{4+} ions only) were used as EPR standards. The EPR study was extended to the Ni-substituted analogues, where both Ni^{2+} and Mn^{4+} are paramagnetic. For $LiMg_{0.5-x}Ni_xMn_{0.5}O_2$ and $Li[Li_{(1-2x)/3}Ni_xMn_{(2-x)/3}]O_2$, an EPR response from Mn^{4+} ions only was detected, while the Ni^{2+} ions remained EPR silent in the frequency range of 9.23–285 GHz. For the diamagnetically diluted oxides, $LiMg_{0.25}Ni_{0.25}Mn_{0.5}O_2$ and $Li[Li_{0.10}Ni_{0.35}Mn_{0.55}]O_2$, two types of Mn^{4+} ions located in a mixed (Mn–Ni–Li)-environment and in a Ni–Mn environment, respectively, were registered by high-field experiments. In the X-band, comparative analysis of the EPR line width of Mn^{4+} ions permits to extract the composition of the first coordination sphere of Mn in layered $LiMg_{0.5-x}Ni_xMn_{0.5}O_2$ ($0 \leqslant x \leqslant 0.5$) and $Li[Li_{(1-2x)/3}Ni_xMn_{(2-x)/3}]O_2$ ($x > 0.2$). It was shown that a fraction of Mn^{4+} are in an environment resembling the ordered "α,β"-type arrangement in $Li_{1-\delta 1}Ni_{\delta 1}[Li_{(1-2x)/3+\delta 1}Ni_{2x/3-\delta 1})_\alpha(Mn_{(2-x)/3}Ni_{x/3})_\beta]O_2$ (where $x = \frac{2}{7}$ and $\delta_1 = 0.06$ were calculated), while the rest of Mn^{4+} are in the Ni,Mn-environment corresponding to the $Li_{1-\delta 2}Ni_{\delta 2}[Ni_{1-y}Mn_y]O_2$ ($y < \frac{1}{2}$) composition with a statistical Ni,Mn distribution. For $Li[Li_{(1-2x)/3}Ni_xMn_{(2-x)/3}]O_2$ with $x \leqslant 0.2$, IR spectroscopy indicated that the ordered α,β-type arrangement is retained upon Ni introduction into monoclinic $Li[Li_{1/3}Mn_{2/3}]O_2$.

Keywords: EPR spectroscopy; Lithium transition metal oxides; Lithium ion batteries

1. Introduction

Lithium–nickel–manganese oxides with layered crystal structure were recently considered as alternative electrode materials for lithium-ion batteries [1–6]. As to well-known layered $LiCoO_2$, X-ray powder diffraction patterns of $LiNi_{0.5}Mn_{0.5}O_2$ were indexed as a trigonal layered structure with space group *R*-3*m* [7]. In addition, up to 10% of Li/Ni mixing was found to proceed between the layers [3,5–7]. However, the structure of lithium–nickel–manganese oxides is still unclear. Based on the careful X-ray diffraction analysis, Dahn et al. have suggested that layered $LiNiO_2$ and monoclinic Li_2MnO_3 oxides form solid solution phases, $Li[Li_{(1-2x)/3}Ni_xMn_{(2-x)/3}]O_2$ at $0 \leqslant x \leqslant 0.5$ [8]. Analysis of the MAS-NMR spectra and lattice imaging by TEM have been interpreted in terms of the structure integration of monoclinic Li_2MnO_3 into layered $LiNiO_2$ leading to complex domain structure of "$LiNiO_2$–Li_2MnO_3" oxides [9].

Recently, computational and spectroscopic techniques have been demonstrated to provide information on local Ni/Mn distribution in the transition metal layers of $LiNi_{0.5}Mn_{0.5}O_2$ [10–14]. Using first principle calculations of stoichiometric $Li[Ni_{0..5}Mn_{0.5}]O_2$, three types of cationic arrangement with close energies were predicted, the "zig-zag" Ni/Mn ordering being the most stable layer configuration (Fig. 1) [10]. ^{6}Li-MAS-NMR analysis clearly shows that Li ions in transition metal layers are preferentially surrounded by Mn, Li–Mn_6 and Li–Mn_5Ni_1 being most favourable configurations [10]. TEM analysis of $Li[Ni_{0.5}Mn_{0.5}]O_2$ with 9% cationic mixing between the layers

*Corresponding author. Fax: +359 2 870 50 24.
E-mail address: radstoy@svr.igic.bas.bg (R. Stoyanova).

0022-4596/$ - see front matter © 2005 Elsevier Inc. All rights reserved.
doi:10.1016/j.jssc.2005.10.038

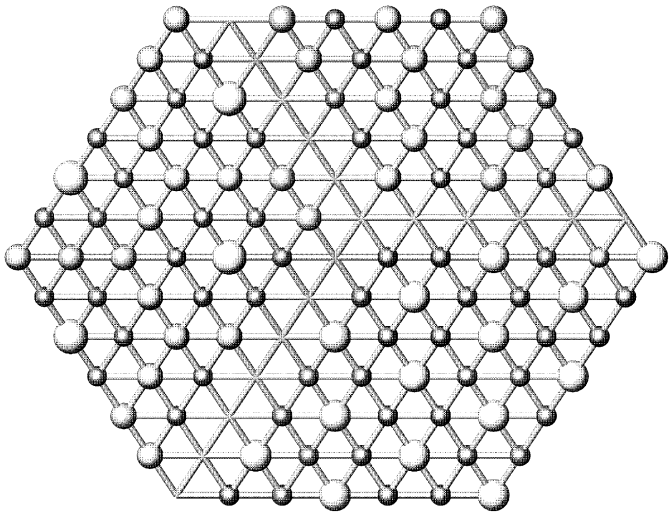

Fig. 1. Schematic presentation of the cationic ordering in $LiNi_{0.5}Mn_{0.5}O_2$: "zig-zag" Ni,Mn ordering (upper right corner), α,β cationic arrangement (down right corner) and "flower"-like cationic configuration (left corner). Small, medium and large balls correspond to manganese, nickel and lithium ions. α,β-sites are denoted by large and small circles.

indicates that Li/Ni and Mn are ordered in the transition metal layer in a way that creates two distinct α- and β-sites forming a $3^{1/2}a \times 3^{1/2}a$ unit cell (Fig. 1) [12]. This type of ordering mimics the cationic distribution of Li/Mn in monoclinic layered $Li[Li_{1/3}Mn_{2/3}]O_3$ ($C2/m$ space group). In order to make the results from TEM and NMR self-consistent, a new type of cationic arrangement (denoted as a "flower"-like pattern) has been suggested by using first-principle electronic structure calculations (Fig. 1) [13]. In this arrangement, each Li is surrounded by a hexagon consisting of Mn, which in its turn is surrounded by a larger hexagon consisting of Ni. Analysis of the local cationic structure in the transition metal oxides by joint NMR and pair distribution function (PDF) [14] have provided evidence that Mn atoms are surrounded mainly by Li and Ni in the first coordination, while Ni atoms tend to be surrounded by more Mn atoms.

The charge compensation in $LiNi_{0.5}Mn_{0.5}O_2$ was found to proceed via Ni^{2+} and Mn^{4+} in the transition metal layers [15]. Magnetic susceptibility measurements of layered $LiNi_{0.5}Mn_{0.5}O_2$ have shown a Curie–Weiss behaviour between 180 and 300 K with a paramagnetic Weiss constant of −92 K [6,16]. No long-range magnetic ordering is achieved at these oxides. The charge distribution and the magnetic properties of $LiNi_{0.5}Mn_{0.5}O_2$ allow examination of the local cationic distribution in the transition metal layers by EPR spectroscopy. Both Ni^{2+} and Mn^{4+} are paramagnetic ions with integer and half-integer spin states, respectively ($S=1$ and $S=\frac{3}{2}$). The conventional EPR spectroscopy (X-band) is best suited for studying the electronic structure of ions with half-integer spin ground states. Contrary, ions with integer spin ground states are usually not active in the X-band due to the higher magnitude of the zero field splitting parameter, D [17]. In this case, EPR spectroscopy at high-frequency and high-fields provides opportunity to apply microwave frequency higher than D and to register these ions [17]. In addition, it is worth to mention that the EPR spectrum of systems containing more than one paramagnetic ion is significantly complicated both at lower- and high-field experiments. However, it has been shown that analysis of the EPR line width (determined at X-band EPR) of Mn^{4+} in ordered $LiMg_xNi_{0.5-x}Mn_{1.5}O_4$ ($0 \leqslant x \leqslant 0.5$) spinels allows differentiating between the contributions of the density of paramagnetic species and the strength of the exchange interactions [18]. Moreover, lithium-transition metal oxides containing more than one paramagnetic ions have been studied by EPR: non-stoichiometric $Li_{1-\delta}Ni_{1+\delta}O_2$ [19–22], layered $LiNi_{1-y}Co_yO_2$ solid solutions [23], $Li_{1-x}Mn_{2-x}O_4$, $LiCo_xMn_{2-x}O_4$ and $LiMg_xNi_{0.5-x}Mn_{1.5}O_4$ spinels [24–29].

The aim of this paper is to study the manganese environment in layered $LiNi_{0.5}Mn_{0.5}O_2$ using conventional and high-frequency EPR spectroscopy (9.203 GHz (X-band), 95 GHz (W-band) and 285 GHz). To rationalize the EPR spectrum of magnetically concentrated systems, we investigate as EPR standards layered oxides where paramagnetic Ni^{2+} ions are replaced by diamagnetic ions. Two kinds of diamagnetic ions are chosen: Li^+ and Mg^{2+}. While the replacement of Ni^{2+} by Li^+ have been reported to yield $Li[Li_{(1-2x)/3}Ni_xMn_{(2-x)/3}]O_2$ solid solutions in whole concentration range [8], there are no data on the isovalent replacement of Ni^{2+} by Mg^{2+}. Amine et al. have reported the preparation of layered Mg-doped oxides, $Li[Ni_{0.475}Mn_{0.475}Mg_{0.05}]O_2$, where Mg substitutes for both Ni and Mn [30]. Following the aim of our investigation, we focused on the preparation of layered $LiMg_{0.5-x}Ni_xMn_{0.5}O_2$ oxides where Mg substitutes for Ni only in a whole concentration range. Taking into account that in mixed oxides the Mg^{2+}/Mn^{4+} and Ni^{2+}/Mn^{4+} cations tend to be arranged in a similar way (for example, $1M^{2+}$:$3Mn^{4+}$ ordering in the octahedral spinel sites of $LiM^{2+}_{0.5}Mn^{4+}_{1.5}O_4$, $M^{2+} \equiv Mg^{2+}$, Ni^{2+} [31]), the newly prepared $LiMg_{0.5}Mn_{0.5}O_2$ composition can be used as an EPR standard for monitoring the local structure of Mn^{4+} in $LiNi_{0.5}Mn_{0.5}O_2$. In addition, it has been shown that Mg dopants have a favourable effect on the stabilization of layered hexagonal structure of $LiMnO_2$ [32,33]. Finally, information on the cationic distribution in $LiNi_{0.5}Mn_{0.5}O_2$ was extracted by comparative analysis of the EPR line width (determined in the X-band) and that of $LiMg_{0.5}Mn_{0.5}O_2$ and $Li[Li_{1/3}Mn_{2/3}]O_3$ containing Mn^{4+} ions only. For the sake of convenience, Mn^{4+} spin probes in layered $LiCoO_2$ were also used as EPR standards. Complimentary to EPR, IR spectra were also recorded.

2. Experimental

2.1. Synthesis and characterization of $LiNi_{0.5-x}Mg_xMn_{0.5}O_2$

$Li[Li_{(1-2x)/3}Ni_xMn_{(2-x)/3}]O_2$ compositions were prepared by a solid state reaction between $LiOH \cdot H_2O$ and

coprecipitated nickel–manganese double hydroxides. The mixture was heated at 480 °C (the temperature of LiOH-melting) for 12 h. The solid residue was homogenized, pelleted and heated at 900 °C for 12 h in air. The same preparation route was used for the synthesis of $LiMg_xNi_{0.5-x}Mn_{0.5}O_2$ compositions, except for the lower synthesis temperature (600 °C) in order to avoid the decomposition of $LiMg_xNi_{0.5-x}Mn_{0.5}O_2$ into MgO and layered Li–Ni–Mn oxides. The lithium content in the samples was determined by atomic absorption analysis. The total content of manganese and nickel was established complexometrically and by atomic absorption analysis. The mean oxidation state of manganese and nickel was determined by iodometric titration.

The X-ray phase analysis was made by a Philips diffractometer with Cu$K\alpha$ radiation. Step-scan recording for structure refinement by the Rietveld method were carried out by using 0.03° 2θ steps of 6 s duration. The computer program FULLPROF was used in the calculations [34]. The diffractometer point zero, Lorentzian/Gaussian fraction of the pseudo-Voigt peak function, scale factor, lattice constants (a and c), oxygen parameter (z), thermal factors for 3a, 3b and 6c positions, half-width parameters, preferred orientation and asymmetry parameters were refined. The Li/(Mn + Ni) and Li/(Mn + Ni + Mg) ratios were imposed by the chemical composition of the oxides. The structural model used comprised Li in 3b sites (000.5), Ni/Mg and Mn in 3a sites (000) and oxygen in 6c sites (00z). The improvement of the fitting procedure was obtained when Li and Ni/Mg were allowed to exchange their positions, δ. The structural model used was in agreement with the previous structural characterization of $Li_{1-\delta}Ni_{\delta}[Li_{\delta}Ni_{0.5-\delta}Mn_{0.5}]O_2$ oxides [7].

The infrared spectra were recorded on a NICOLET AVATAR-320 spectrometer in KBr pellets.

The EPR spectra were recorded as a first derivative of the absorption signal of an ERS-220/Q (ex-GDR) spectrometer within the temperature range of 90–400 K. The g-factors were determined with respect to a Mn^{2+}/ZnS standard. The signal intensity was established by double integration of the experimental EPR spectrum. The high-frequency EPR spectra were recorded at a single-pass transmission EPR spectrometer built in the High-Magnetic Filed Laboratory, Grenoble, France. The frequencies were changed from 95 to 475 GHz using Gunn diodes and their multipliers. Absorption were detected with an bolometer. The recording temperatures were varied between 5 and 300 K using a variable temperature insert (Oxford Instruments).

2.2. Analysis of the EPR line width in magnetically concentrated systems

In magnetically concentrated systems, dipole–dipole, M_{dd}^2, and exchange interactions, H_e, between "allied" paramagnetic spins contribute additionally to the EPR line width as compared to the line width of isolated spins [35–37], which are expressed by

$$\Delta H_{pp} = \text{const}\frac{M_{dd}^2}{H_e} = \text{const}\frac{g^2 S(S+1)\sum_{i,k}(1-3\cos^2\Theta_{ik})/r_{i,k}^6}{\sqrt{\frac{8}{3}S(S+1)zJ}}, \quad (1)$$

where z, $r_{i,k}$ and $\Theta_{i,k}$ denote the number of paramagnetic nearest neighbours particles, the distance between them and the angle of the radius vector between two spins with the magnetic field, respectively; J corresponds to the strength of exchange interactions. In the case of polycrystalline samples, the average angular term is $\frac{4}{5}$. For a trigonal layer, the first, second and third metal neighbours will contribute by 95.0%, 3.5% and 1.5%, respectively, to the line width. As a first approximation, this allows restriction of the dipole–dipole contribution up to the first neighbours. In order to rationalize this formula, the exchange term can be replaced the experimentally accessible Weiss constant, $\Theta = \frac{2}{3}S(S+1)zJ/k$

$$\Delta H_{pp} = \text{const}\, g^2\beta^2\frac{\{S(S+1)\}^{3/2}z^{3/2}}{r^6\Theta}. \quad (2)$$

It is important to mention that the Weiss constant represents the average sum of exchange interactions on an atomic site $\Theta = \frac{2}{3}S(S+1)z\sum J_i/k$. Therefore, Eq. (2) can be used experimentally when antiferro- or ferromagnetic interactions on atomic site are dominant [18]. The comparative analysis of the EPR line with respect to a composition with already known EPR parameters (which will be denoted further on as "EPR standard") allows estimating the mean number of paramagnetic species around the EPR active center:

$$z = \left\{ z_{st}^{3/2}\frac{(\Delta H_{pp}\Theta)}{(\Delta H_{pp}\Theta)_{st}}\left(\frac{g_{st}}{g}\right)^2\left(\frac{r_{st}}{r}\right)^{-6}\right\}^{2/3}. \quad (3)$$

Contrary to the effect of the "allied" paramagnetic ions, the effect of "alien" paramagnetic spins on the EPR line width is theoretically not well described. However, it has been demonstrated for ordered $LiMg_xNi_{0.5-x}Mn_{1.5}O_4$ spinels that Eq. (1) becomes also valid in the case of alien paramagnetic species, when a term, F(alien), taking into account the dipole–dipole and exchange interactions is included [18]:

$$\Delta H_{pp} = \text{const}\frac{M_{dd}^2(\text{allied}) + F(\text{alien})}{H_e(\text{allied})}. \quad (4)$$

3. Results and discussion

3.1. XRD and IR characterization of $LiNi_{0.5-x}Mg_xMn_{0.5}O_2$

The hydroxide synthesis procedure yields "XRD pure" $LiMg_{0.5-x}Ni_xMn_{0.5}O_2$ phases in the whole concentration

range of x, $0 \leqslant x \leqslant 0.5$ (Fig. 2). Analysis of the XRD patterns shows that the layered crystal structure is preserved upon Mg substitution. Fig. 3 gives the concentration dependence of the unit cell parameters. For the sake of comparison, the same figure presents the variation of the unit cell parameters for $Li[Li_{(1-2x)/3}Ni_xMn_{(2-x)/3}]O_2$ compositions. (To compare the effect of Li and Mg substituents on the unit cell dimensions, the XRD patterns of $Li[Li_{(1-2x)/3}Ni_xMn_{(2-x)/3}]O_2$, $0.2 > x > 0$, and monoclinic $Li[Li_{1/3}Mn_{2/3}]O_2$ are indexed in the R-3m space group.) The replacement of Ni by Mg leads to an expansion of the unit cell dimensions, whereas an unit cell contraction is observed with Li substitution. Rietveld analysis of the XRD patterns of $LiMg_{0.5-x}Ni_xMn_{0.5}O_2$ shows that the replacement of Ni by Mg favours the cationic mixing between the layers, which is contrary to that observed for Li substituted oxides (Fig. 3). In addition, the peak widths for $LiMg_{0.5}Mn_{0.5}O_2$ are higher as comparison with that for

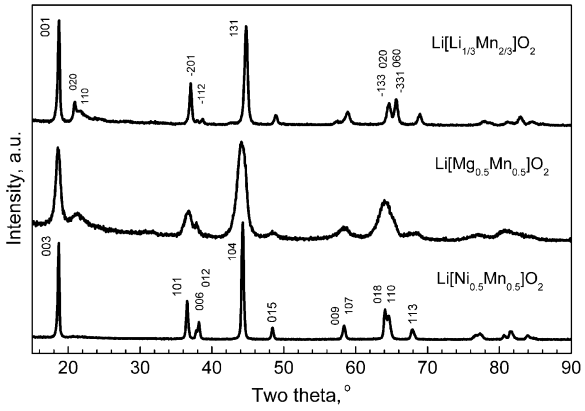

Fig. 2. XRD patterns of $Li[Li_{1/3}Mn_{2/3}]O_2$, $LiMg_{0.5}Mn_{0.5}O_2$ and $LiNi_{0.5}Mn_{0.5}O_2$ compositions. The indexing of the most intensive reflections for R-3m and $C2/m$ space group are also given.

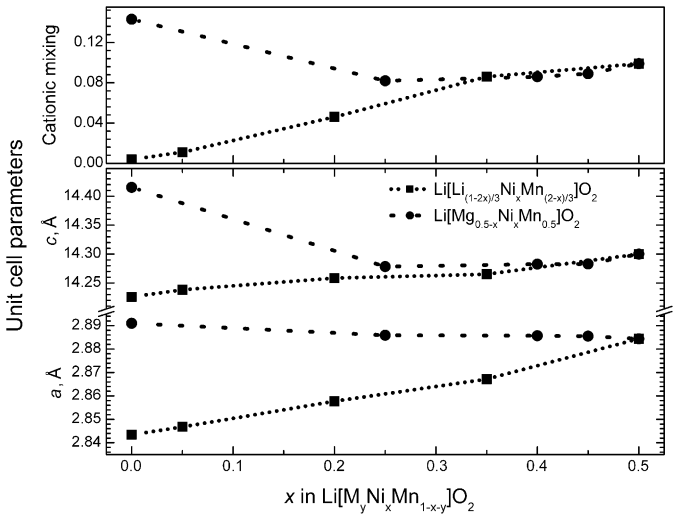

Fig. 3. Unit cell dimensions (a and c) and the amount of Ni,Mg ions residing in the lithium layers (cationic mixing) Versus the Ni content in $LiMg_{0.5-x}Ni_xMn_{0.5}O_2$ and $Li[Li_{(1-2x)/3}Ni_xMn_{(2-x)/3}]O_2$.

$LiNi_{0.5}Mn_{0.5}O_2$ (Fig. 2). However, there is no selective broadening of the XRD diffraction lines. This means that particle sizes contribute to the XRD diffraction lines of $LiMg_{0.5}Mn_{0.5}O_2$. It is worth to mention that pure $LiMg_{0.5}Mn_{0.5}O_2$ phase can be obtained at 600 °C only, while 900 °C is needed for the preparation of $LiNi_{0.5}Mn_{0.5}O_2$.

IR spectroscopy has been shown to be an effective experimental tool for studying the cationic ordering in complex compositions, even in cases when it is not accessible by XRD techniques [31,38]. Fig. 4 compares the IR spectra of $Li[Mg_{0.5-x}Ni_xMn_{0.5}]O_2$ and $Li[Li_{(1-2x)/3}Ni_xMn_{(2-x)/3}]O_2$ compositions in the 400–850 cm^{-1} region, where only the vibrations of $[Mg_{0.5-x}Ni_xMn_{0.5}]O_2$ and $[Li_{(1-2x)/3}Ni_xMn_{(5-x)/3}]O_2$ are visible. Between 400 and 800 cm^{-1}, the IR spectrum of $Li[Li_{1/3}Mn_{2/3}]O_3$ displays a broad band with fine structure, which reflects the Li/Mn ordering in the ($LiMn_2$)-layers also detected by XRD technique (Fig. 4A). The fine structure of the IR band is preserved upon Ni substitution for Li up to Li/Ni = 1, $Li[Li_{0.2}Ni_{0.2}Mn_{0.6}]O_2$. This result means that α,β-arrangement is retained upon Ni introduction in monoclinic $Li[Li_{1/3}Mn_{2/3}]O_2$. Further increase in the Ni content leads to a broadening of the fine structure lines, culminating for the $LiNi_{0.5}Mn_{0.5}O_2$ composition in two intense modes at 585 and 520 cm^{-1} with a shoulder at 475 cm^{-1}. The broadening of the IR modes, as well as the loss of the fine structure can be related to the increased amount of Li and Ni ions exchanged between the layers in the Ni-rich compositions, $Li_{1-\delta}Ni_\delta[Li_\delta Ni_{0.5-\delta}Mn_{0.5}]O_2$ (Fig. 4A). The effect of the cationic mixing on the IR profile is well demonstrated with non-stoichiometric $Li_{1-\delta}Ni_{1+\delta}O_2$ compositions: by increasing the Ni amount in the Li site the two characteristic IR modes merge into one featureless band [39]. Therefore, the cationic mixing between the layers creates difficulties in the interpretation of the Ni/Mn distribution in $[Li_\delta Ni_{0.5-\delta}Mn_{0.5}]O$-layers using IR spectroscopy only.

The mutual effect of the cationic ordering in the layers and the cationic mixing between the layers can be followed in the IR spectra of Mg substituted $Li[Ni_{0.5}Mn_{0.5}]O_2$ (Fig. 4B).When Mg substitutes for Ni, the number of the IR modes increases, culminating with the end composition $LiMg_{0.5}Mn_{0.5}O_2$ in a resolved IR band structure. It is important to mention that $LiMg_{0.5}Mn_{0.5}O_2$, characterized also with a higher degree of cationic mixing between layers, displays the structured IR profile. Close inspection of the diffuse and structured IR spectra of Ni- and Mg-rich compositions shows similar IR profiles, thus indicating a similar Ni/Mn and Mg/Mn distribution in the layer.

3.2. EPR spectroscopy of $Li[Ni_{0.5-x}Mg_xMn_{0.5}]O_2$

Fig. 5 compares the EPR spectra of $Li[Li_{1/3}Mn_{2/3}]O_2$ and $Li[Mg_{0.5}Mn_{0.5}]O_2$ compositions. For ordered $Li[Li_{1/3}Mn_{2/3}]O_2$, it has been found that the antiferromagnetically coupled Mn^{4+} ions account for the appearance of an EPR signal with Lorentzian line shape and $g = 1.9955$ [40,41]. In

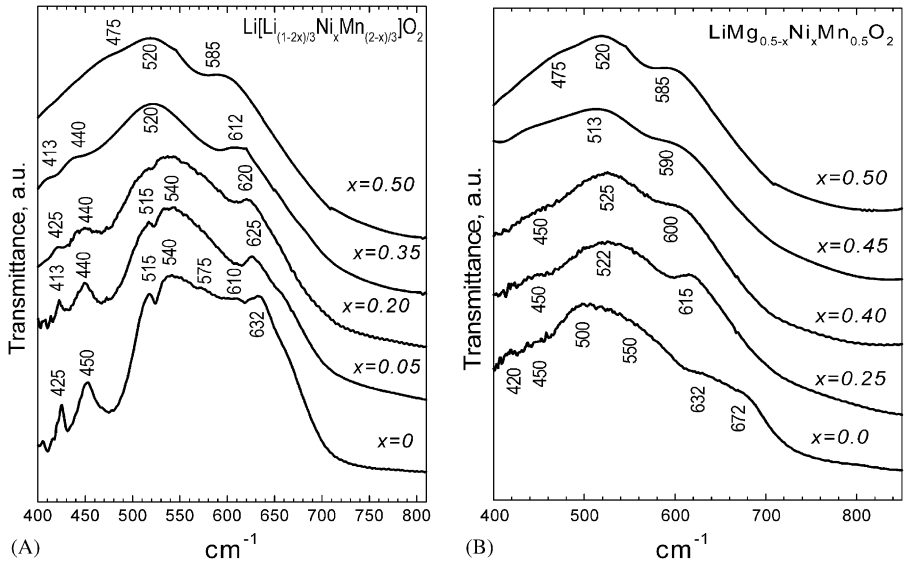

Fig. 4. IR spectra of $Li[Li_{(1-2x)/3}Ni_xMn_{(2-x)/3}]O_2$ (A) and $LiMg_{0.5-x}Ni_xMn_{0.5}O_2$ (B).

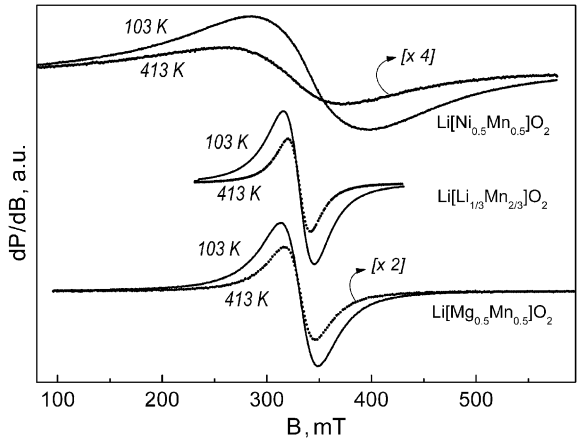

Fig. 5. X-band EPR spectra of $LiMg_{0.5}Mn_{0.5}O_2$, $Li[Li_{1/3}Mn_{2/3}]O_2$ and $LiNi_{0.5}Mn_{0.5}O_2$ compositions.

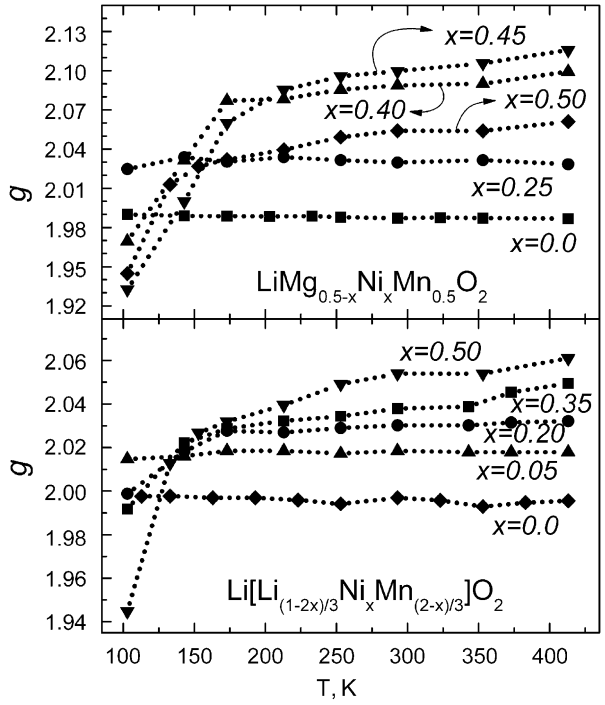

Fig. 6. Temperature variation in the g-factor of Mn^{4+} ions in $Li[Li_{(1-2x)/3}Ni_xMn_{(2-x)/3}]O_2$ and $LiMg_{0.5-x}Ni_xMn_{0.5}O_2$. The EPR spectra were recorded at 9.23 GHz (X-band).

comparison with ordered $Li[Li_{1/3}Mn_{2/3}]O_2$, the EPR spectrum of the new $Li[Mg_{0.5}Mn_{0.5}]O_2$ phase also consists of a Lorentzian line with $g = 1.989$, which allows one to assign this signal to exchange coupled Mn^{4+} ions again. The temperature variation in the signal intensity follows the Curie–Weiss behaviour with a Weiss constant $\Theta = +25$ K, indicating ferromagnetic interactions between the Mn^{4+} ions. For ordered $Li[Li_{1/3}Mn_{2/3}]O_2$, the Weiss constant determined from the temperature variation of the EPR signal intensity is -44 K. The observed ferro- and antiferromagnetic interactions in $Li[Mg_{0.5}Mn_{0.5}]O_2$ and $Li[Li_{1/3}Mn_{2/3}]O_2$, respectively, can be explained if we take into account the distance between the Mn^{4+} ions. For Mn^{4+}-containing spinel oxides, it is well known that the ferromagnetic interactions are dominant at a distance, r, between the Mn^{4+} ions exceeding 2.87 Å, while the antiferromagnetic interactions are more stronger at $r < 2.87$ Å [42–44]. This is what we observe for $Li[Li_{1/3}Mn_{2/3}]O_2$ and $Li[Mg_{0.5}Ni_{0.5}]O_2$: $r = 2.843$ and 2.891 Å, respectively.

Following the classical EPR notation, there will be no EPR response from magnetically concentrated oxides containing more than one kind of paramagnetic species. However, after replacing diamagnetic Mg^{2+} or Li^+ by paramagnetic Ni^{2+}, a single line with Lorentzian shape is still observable in the X-band EPR spectra of $Li[Li_{(1-2x)/3}Ni_xMn_{(2-x)/3}]O_2$ and $Li[Mg_{0.5-x}Ni_xMn_{0.5}]O_2$ compositions

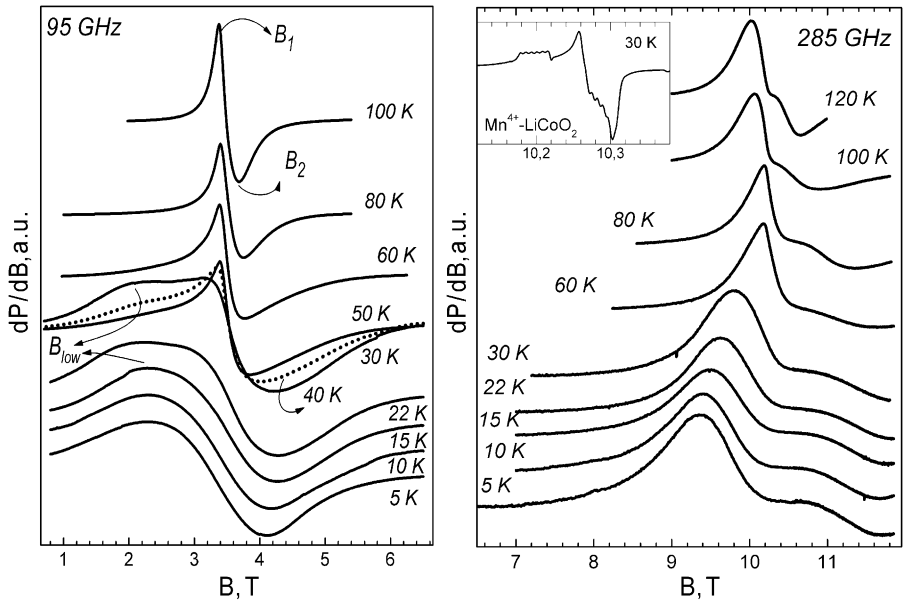

Fig. 7. EPR spectra at 95 GHz (left) and 285 GHz (right) of $LiNi_{0.5}Mn_{0.5}O_2$. The apparent g_1, g_2 and average g_{ave} (corresponding to the resonance field B_1, B_2, B_{ave}), as well as the low-magnetic field absorption, B_{low}, are indicated. The inset shows the EPR spectrum at 285 GHz of Mn^{4+} spin probes in $LiCoO_2$.

(Fig. 5). The g-factor depends on both Ni-content and registration temperature (Fig. 6). At 413 K, the g-factor increases slightly with the Ni-content. On cooling from 413 to 103 K, there is a decrease in the g-factor (Fig. 6). The observed variation in the g-factor with the Ni-content is not sensitive towards the appearance of Li^+ or Mg^{2+} in the oxide compositions.

In order to gain insight into the signal origin at $LiNi_{0.5}Mn_{0.5}O_2$, high-frequency EPR spectroscopy (at 95 and 285 GHz) was carried out. It is worth to mention that, for ions with half-integer spin states, high-field experiments allow resolving small g-tensor anisotropies which is not accessible by X-band experiments [45]. Fig. 7 shows the high-frequency EPR spectra of $LiNi_{0.5}Mn_{0.5}O_2$ in the temperature range of 5–100 K. At 100 K, the high-frequency EPR spectrum of $LiNi_{0.5}Mn_{0.5}O_2$ consists of a signal with tetragonal symmetry, while the single Lorentzian line is observed in the X-band (Fig. 7). Between 100 and 60 K, the apparent g_2 and g_1 factors of high-frequency EPR signal are slightly dependent on whether 95 or 285 GHz is used. It is important that the average g-value ($g_{ave} = 2/3g_1 + 1/3g_2$) tends to the isotropic g-factor determined in X-band (Fig. 8). This result indicates that EPR response from $LiNi_{0.5}Mn_{0.5}O_2$ detected at lower and higher magnetic fields has one and the same origin. For the sake of comparison, Fig. 7 shows the EPR spectrum of Mn^{4+} spin probes in $LiCoO_2$. It is worth mentioning that the perpendicular component determined at 95 and 285 GHz, g_1, has the value close to the perpendicular component of Mn^{4+} in $LiCoO_2$, while the parallel component is different (Table 1). Below 60 K, there are a line broadening and a strong resonance shift. In this temperature range, low- and high-magnetic field resonance absorptions are superimposed on the main resonance

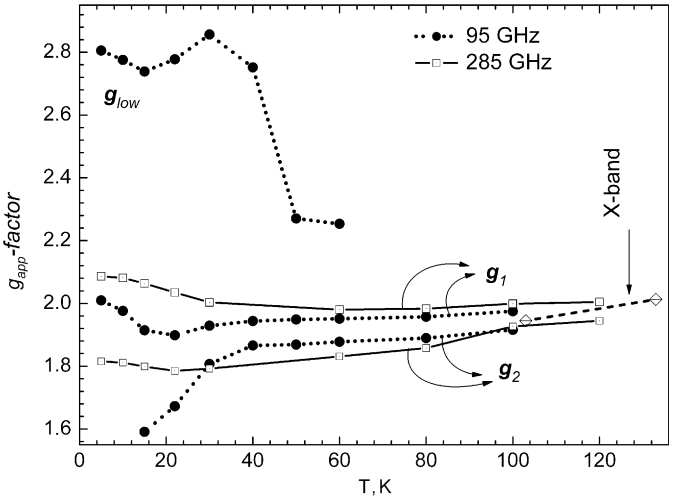

Fig. 8. Temperature variation in the apparent g_1, g_2 and g_{low} factors of $LiNi_{0.5}Mn_{0.5}O_2$. The EPR spectra are registered at 95 GHz.

signal, indicating the transition from localized to magnetically correlated spins (Fig. 7). At 285 GHz, the changes in low- and high-magnetic field resonance absorptions are suppressed as compared to that at 95 GHz. This can be related with the saturation of the magnetization in high-fields applied at 285 GHz. The transition of the EPR spectrum from localized to magnetically correlated spins have already been reported for non-stoichiometric $Li_{1-\delta}Ni_{1+\delta}O_2$, where Ni^{2+} in the Li-site (created strong 180°-magnetic interactions with Ni ions in the nickel layers) were responsible for observed EPR changes below 210 K [19–22]. For $LiNi_{0.5}Mn_{0.5}O_2$, the EPR spectrum from magnetically correlated spins can therefore be associated with the effect of Ni^{2+} residing the Li-site in $LiNi_{0.5}$

Table 1
The g-factor of single Lorentzian line detected at X-band (g_{single}), g-factor of the symmetrical line detected at 95 GHz (g_{sym}) and apparent g_1 and g_2 detected at 95 and 285 GHz for $LiNi_{0.5}Mn_{0.5}O_2$, $LiLi_{0.10}Ni_{0.35}Mn_{0.55}O_2$ and $LiMg_{0.25}Ni_{0.25}Mn_{0.5}O_2$

Samples	X-band	95 GHZ			285 GHz	
	g_{single} (± 0.008)	g_{sym} (± 0.004)	g_1 (± 0.004)	g_2 (± 0.004)	g_1 (± 0.001)	g_2 (± 0.001)
$LiNi_{0.5}Mn_{0.5}O_2$	1.945	Not observed	1.975	1.916	1.999	1.927
$LiLi_{0.10}Ni_{0.35}Mn_{0.55}O_2$	1.992	2.044	1.962	1.908	2.011	1.932
$LiMg_{0.25}Ni_{0.25}Mn_{0.5}O_2$	2.025	2.053	1.979	1.949		
Mn^{4+}–$LiCoO_2$[a]			1.9778	1.9972	1.9778	1.9972

For the sake of comparison, the g-tensor ($g_\perp$ and $g_\parallel$) for Mn^{4+} spin probes in $LiCoO_2$ is also given.
[a]The accuracy in the determination of the g-tensor is 0.0002.

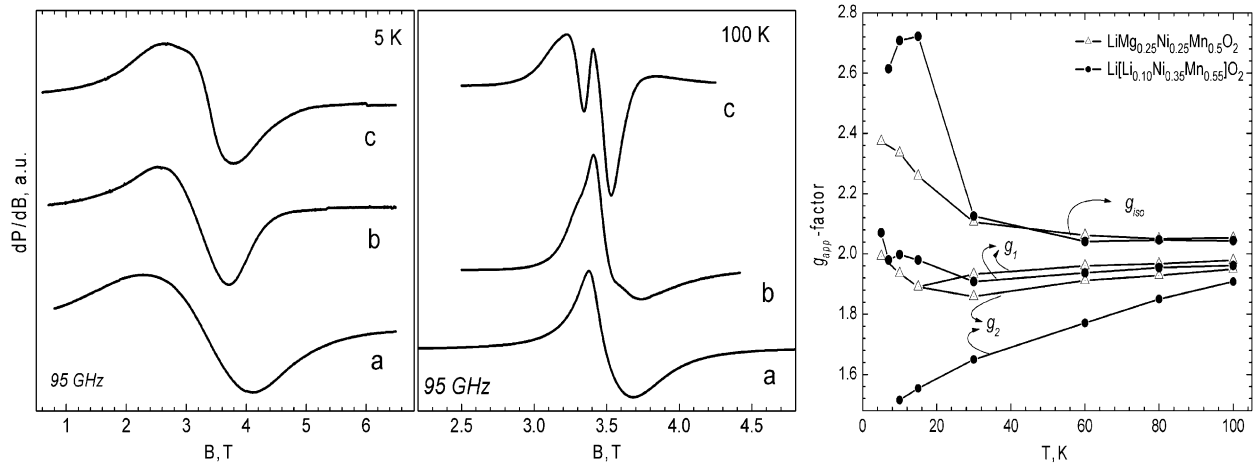

Fig. 9. High-frequency EPR spectra at 100 and 5 K of $LiNi_{0.5}Mn_{0.5}O_2$ (a), $Li[Li_{0.10}Ni_{0.35}Mn_{0.55}]O_2$ (b) and $LiMg_{0.25}Ni_{0.25}Mn_{0.5}O_2$ (c). Temperature variation in the apparent g_1, g_2 and g_{iso} factors for $Li[Li_{0.10}Ni_{0.35}Mn_{0.55}]O_2$ and $LiMg_{0.25}Ni_{0.25}Mn_{0.5}O_2$.

$Mn_{0.5}O_2$. In addition, the EPR experiments demonstrate that long magnetic order is not achieve at $LiNi_{0.5}Mn_{0.5}O_2$ even at 5 K.

At 100 K, the anisotropic EPR response was also detected for the Li and Mg-substituted oxides, $Li[Li_{0.1}Ni_{0.35}Mn_{0.55}]O_2$ and $Li[Mg_{0.25}Ni_{0.25}Mn_{0.5}]O_2$ (Fig. 9A). The temperature variation of the apparent g_2 and g_1 factors are given in Fig. 9B. While the perpendicular component observed for $Li[Li_{0.1}Ni_{0.35}Mn_{0.55}]O_2$ and $Li[Mg_{0.25}Ni_{0.25}Mn_{0.5}]O_2$ match with that for $LiNi_{0.5}Mn_{0.5}O_2$, the parallel component is different (Table 1). Contrary to $LiNi_{0.5}Mn_{0.5}O_2$, the average g-value does not agree with the isotropic g-factor determined in the X-band.

In addition, Mg-substituted oxide displays at 100 K an additional symmetrical signal with $g = 2.053$ and line width of 200 mT. The same signal with lower intensity was also observed in the EPR spectrum of $Li[Li_{0.1}Ni_{0.35}Mn_{0.55}]O_2$. Between 100 and 60 K, the g-factor remains the same, while, below 60 K, g increases. The g-factor of the symmetrical signal is not consistent with the g-factor of the isotropic signal detected at X-band. However, the g-factor determined in the X-band is close to the average value calculated from the g-factors of the main anisotropic and additional symmetrical signals determined at 95 GHz. This means that high-fields experiments lead to the splitting of the isotropic signal detected at lower magnetic fields.

Comparison of the high-frequency EPR spectra of $Li[Li_{0.1}Ni_{0.35}Mn_{0.55}]O_2$, $Li[Mg_{0.25}Ni_{0.25}Mn_{0.5}]O_2$ and $LiNi_{0.5}Mn_{0.5}O_2$ compositions with the EPR spectrum of Mn^{4+} spin probes in $LiCoO_2$ permits to attribute the anisotropic EPR signal to Mn^{4+} ions. The close value of the perpendicular component shows similar Mn^{4+}-environment in $Li[Li_{0.1}Ni_{0.35}Mn_{0.55}]O_2$, $Li[Mg_{0.25}Ni_{0.25}Mn_{0.5}]O_2$ and $LiNi_{0.5}Mn_{0.5}O_2$ compositions. It appears that the paramagnetic Ni^{2+} ions are not EPR active even in the higher frequency used. This fact can be understood if we consider the spin–spin relaxation of Ni^{2+} and Mn^{4+}. Due to the different electronic configuration, the Ni^{2+} ions have a shorter spin–spin relaxation time as compared to that of Mn^{4+}. The fast fluctuating field created by the Ni^{2+} spins promotes an effective interaction of the Mn^{4+} spins with the lattice, thus leading to the possibility of registering an EPR signal from Mn^{4+}. However, the presence of Ni^{2+} in the proximity of Mn^{4+} can be related both with an inhomogeneous broadening of the EPR signal detected at high-magnetic fields (95 and 285 GHz) and a homogeneous broadening in lower magnetic fields (9.23 GHz).

For diamagnetically diluted $Li[Li_{0.1}Ni_{0.35}Mn_{30.55}]O_2$ and $Li[Mg_{0.25}Ni_{0.25}Mn_{0.5}]O_2$, the g-factor of the additional symmetrical signal detected at higher magnetic fields is not consistent with that typical for Ni^{2+} or Ni^{3+} ions [17,19]. The positive deviation of the g-factor of the additional symmetrical signal from the g-factor of the free electron can tentatively be associated Mn^{4+} ions located in paramagnetic Ni-rich environment. The broadening of the EPR signal of $LiNi_{0.5}Mn_{0.5}O_2$ does not permit to observe the additional symmetrical signal. At lower magnetic fields (9.23 GHz), all EPR signals are merged into one signal.

3.2.1. EPR study of the cationic distribution in $Li[Ni_{0.5-x}Mg_xMn_{0.5}]O_2$

To determine the local cationic distribution in Mn^{4+}-containing layered oxides, comparative analysis of the EPR line width of exchange coupled Mn^{4+} ions in X-band EPR was carried out according to Eq. (3). For both $Li[Li_{1/3}Mn_{2/3}]O_2$ and $Li[Mg_{0.5}Mn_{0.5}]O_2$, the EPR line width increases weakly on cooling from 413 K (Fig. 10). The line width of $Li[Mg_{0.5}Mn_{0.5}]O_2$, determined at 413 K, is slightly higher than that for ordered $Li[Li_{1/3}Mn_{2/3}]O_2$: 29.8 and 21.3 mT, respectively. The Weiss constant change from -44 to $+25$ K when changing from $Li[Li_{1/3}Mn_{2/3}]O_2$ to $Li[Mg_{0.5}Mn_{0.5}]O_2$. Having in mind that the first metal shell of Mn^{4+} in $Li[Li_{1/3}Mn_{2/3}]O_2$ consists of 3 Mn^{4+} and 3 Li^+ [46], we have calculated from Eq. (3) the mean number of paramagnetic ions around Mn^{4+} in $Li[Mg_{0.5}Mn_{0.5}]O_2$: $z = 2.6$. This value will be lower if we suppose a random Mg and Mn distribution in the layer: $z = 3$.

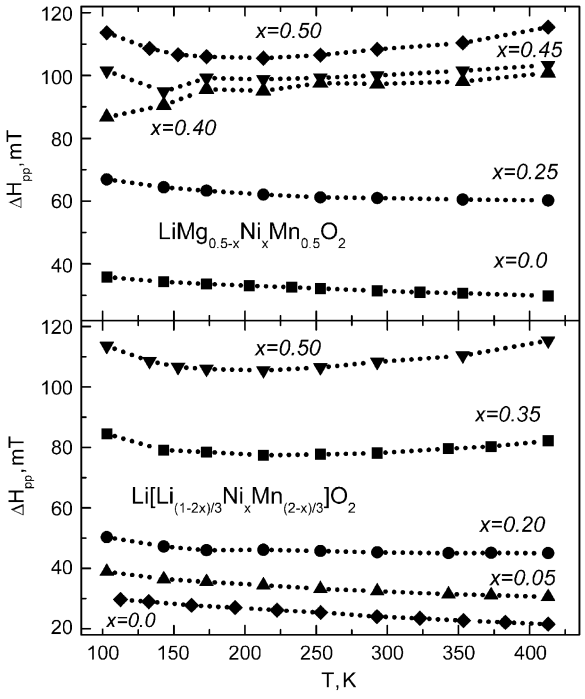

Fig. 10. Temperature variation in the EPR line width of Mn^{4+} ions in $Li[Li_{(1-2x)/3}Ni_xMn_{(2-x)/3}]O_2$ and $LiMg_{0.5-x}Ni_xMn_{0.5}O_2$. The EPR spectra were recorded at 9.23 GHz (X-band).

As already mentioned in the Introduction, three types of cationic arrangements are considered for $Li[Ni_{0.5}Mn_{0.5}]O_2$, which can be distinguished in respect of the composition of the first metal shell of Mn^{4+} (Fig. 1). In the "zig-zag" configuration, each Mn^{4+} has 2 Mn^{4+} and 4 Ni^{2+} as first metal neighbours [10]. In the "α,β"-arrangement, each Mn^{4+} is surrounded by 3 β-site ions (Mn^{4+} and Ni^{3+}) and 3 α-site ions (Ni^{2+} and Li^+) with Mn^{4+} mean number of 2.25 in the first metal shell [12]. The "flower"-like cationic configuration is identical with the "zig-zag" one with respect to the amount of Mn^{4+} ions acting as first metal neighbours: each Mn^{4+} has 1 Li^+, 3Ni^{2+} and 2 Mn^{4+} ions in the first metal shell [14]. Since $Li[Mg_{0.5}Mn_{0.5}]O_2$ and $Li[Ni_{0.5}Mn_{0.5}]O_2$ are isostructural, the same cationic ordering can be supposed for both compositions. As one can see, the experimentally determined value of the mean number of paramagnetic neighbours of Mn^{4+} in $Li[Mg_{0.5}Mn_{0.5}]O_2$ approximates to that of "α,β"-arrangement. This indicates that "α,β"-type cationic arrangement with some extent of local disorder describes the Li^+, Mg^{2+} and Mn^{4+} distribution in $[Li_\delta Mg_{0.5-\delta}Mn_{0.5}]O_2$-layers.

Therefore, we propose another model for Li, Mg and Mn-distribution in the $[Li_\delta Mg_{0.5-\delta}Mn_{0.5}]O_2$-layers. This model is based on several experimental observations: (i) "α,β"-type cationic arrangement is valid in the concentration range of $0 \leqslant x < 0.35$ for $Li[Li_{(1-2x)/3}Ni_xMn_{(2-x)/3}]O_2$ (IR spectroscopy); (ii) appearance of cationic disorder in the "α,β"-type cationic arrangement for $x > 0.35$ (EPR); (iii) detection in the HF-EPR spectrum of two types of Mn^{4+} ions in diamagnetically diluted layered oxides, and (vi) Li atoms in the transition metal layers are surrounded preferentially by five or more Mn atoms and no more 1 Ni atom (Li NMR [10]). According to this model, one part of Mn^{4+} ions are located in the environment which mimics the "α,β"-type arrangement established with $Li[Li_{(1-2x)/3}Ni_xMn_{(2-x)/3}]O_2$ ($x < 0.35$), while the rest of Mn^{4+} ions occupy Ni-rich position. To evaluate the mean number of Mn^{4+} there is a need to determine the composition of the environment that mimics the "α,β"-type arrangement. Based on the solid state Li NMR analysis, the composition can be derived from the requirements that Li will have the equal probability to contact with 6 Mn atoms or with 5 Mn and 1 Ni atoms. Supposing the random distribution of ions in the α- and β-site of $Li[(Li_{(1-2x)/3}Ni_{2x/3})_\alpha (Mn_{(2-x)/3}Ni_{x/3})_\beta]O_2$, the probability of Li to have (6-n) Mn and n Ni atoms (from the β-site) can be expressed by Bernouillian statistical distribution: $P(x,n) = C_6^n * (2-x)/2)^{6-n}(x/2)^n$. For the composition with $x = \frac{2}{7}$, the probability of Li atoms to have 6 Mn is equal to the probability of Li to have 5 Mn and 1 Ni. The characteristic feature of layered $Li[Li_{(1-2x)/3}Ni_xMn_{(2-x)/3}]O_2$ is the cationic mixing between layers due to the close ionic dimensions of Li^+ and Ni^{2+}: 0.76 and 0.69 Å, respectively. Since the cationic mixing for compositions with $x = 0.2$ and 0.35 is 0.046 and 0.083, respectively, we include the average value for the cationic mixing at the estimated composition with $x = \frac{2}{7}$: $\delta = 0.06$. Finally, we obtain the following composition:

$Li_{1-\delta}Ni_{\delta}[(Li_{3/21+\delta}Ni_{4/21-\delta})_{\alpha}(Mn_{12/21}Ni_{2/21})_{\beta}]O_2$ where $\delta = 0.06$ and $Li/Ni = \frac{1}{2}$.

Using this model, the Mn^{4+}-environments in the $Li_{1-\delta}Mg_{\delta}[Li_{\delta}Mg_{0.5-\delta}Mn_{0.5}]O_2$ standard can be described by two discrete compositions:

$$\frac{7\delta}{(1+7\delta_1)}Li_{1-\delta_1}Mg_{\delta_1}[(Li_{3/21+\delta_1}Mg_{4/21-\delta_1})_{\alpha}(Mn_{12/21}Ni_{2/21})_{\beta}]O_2$$

with an ordered α,β-type arrangement, and

$$\left\{1-\frac{7\delta}{(1+7\delta_1)}\right\}Li_{1-\delta_2}Mg_{\delta_2}[Mg_{1/2+\delta(1-6\delta_1)/(1-7\delta+7\delta_1-6\delta\delta_1)}Mn_{1/2-\delta(1-6\delta_1)/(1-7\delta+7\delta_1-6\delta\delta_1)}]O_2$$

with a statistical Ni,Mn-distribution. Here δ corresponds to the experimentally obtained value of the cationic mixing between the layers ($\delta = 0.13$), δ_1 denotes the calculated one ($\delta_1 = 0.06$), and δ_2 is expressed by δ and δ_1 as follows: $\delta_2 = \delta/(1-7\delta+7\delta_1)$. This means that 65% of the Mn^{4+} ions will have $\frac{18}{7}Mn^{4+}$ and $\frac{3}{7}Ni^{2+}$ from the β-site and $(\frac{9}{7}+9\delta_1)$ Li^{+} and $(\frac{12}{7}-9\delta_1)$ Ni^{2+} from the α-site, while 35% of Mn^{4+} will be surrounded by $(3+6\delta(1-6\delta_1)/(1-7\delta+7\delta_1-6\delta\delta_1))$ Mg^{2+} and $(3-6\delta(1-6\delta_1)/(1-7\delta+7\delta_1-6\delta\delta_1))$ Mn^{4+} ions. By substituting, the average number of metal neighbours around Mn^{4+} in $Li_{0.87}Mg_{0.13}[Li_{0.13}Mg_{0.37}Mn_{0.5}]O_2$ will be: $2.32Mn^{4+}$, $2.49Mg^{2+}$ and $1.19Li^{+}$. There is a better agreement with the experimentally obtained value: $z = 2.6$.

The same model was applied for Ni containing analogues, $Li[Ni_{0.5-x}Mg_xMn_{0.5}]O_2$ and $Li[Li_{(1-2x)/3}Ni_xMn_{(2-x)/3}]O_2$. Fig. 10 gives the effect of Ni^{2+} ions on the EPR line width of Mn^{4+} between 413 and 103 K. The results obtained clearly reveal the broadening effect of the Ni^{2+} ions in whole temperature range. Adapting the method of moments (Eq. (4)), the EPR line width of Mn^{4+} for nickel-containing oxides is normalized as compared to that of pure Mn^{4+}-containing oxides ($LiMg_{0.5}Mn_{0.5}O_2$ or $Li[Li_{1/3}Mn_{2/3}]O_2$ for both series of compositions):

$$\frac{\Delta H_{pp}}{\Delta H^{o}_{pp}} = 1 + \frac{F(\text{alien})}{M^2_{dd}(\text{allied})}. \quad (5)$$

Suggesting that F(alien) depends on the amount of Ni and M^2_{dd}(allied) is a function of the Mn-amount, then one can expect the linear dependence of the normalized line width on the [Ni]/[Mn]-ratio.

For the first series comprising $Li[Li_{(1-2x)/3}Ni_xMn_{(2-x)/3}]O_2$ with $0 \leqslant x \leqslant 0.2$, the local Ni to Mn ratio was estimated in the framework of the "α,β"-type cationic arrangement. Thus, the first coordination sphere of Mn^{4+} in the transition metal layers will include $1.5*(2-x)$Mn and $1.5x$Ni from the β-site and $3*(1-2x+3\delta)$Li and $3*(2x-3\delta)$Ni from the α-site. Of importance is that the cationic mixing, δ, affects the occupancy of the α-site only, while the occupancy of the β-site remains the same. While the cationic mixing between lithium and transition metal layers for $LiMg_{0.5}Mn_{0.5}O_2$ standard has no effect on the EPR line width of Mn^{4+}, the appearance of paramagnetic Ni^{2+} ions in the lithium layers (three nearest ions in up- and down-layers, respectively) has also to be included in the local environment of the Mn^{4+} ions for $Li[Li_{(1-2x)/3}Ni_xMn_{(2-x)/3}]O_2$ series ($0 \leqslant x \leqslant 0.2$).

For the second series comprising $Li[Mg_{0.5-x}Ni_xMn_{0.5}]O_2$ and $Li[Li_{0.1}Ni_{0.35}Mn_{0.55}]O_2$, the local Ni to Mn ratio was estimated by applying the same model as $LiMg_{0.5}Mn_{0.5}O_2$ standard, where the random Ni^{2+}/Mg^{2+} distribution is supposed. In this case two types of Mn^{4+} ions appear in the transition metal layers: one part of Mn^{4+} are in the environment resembling the α,β-type arrangement of estimated $Li_{1-\delta_1}Ni_{\delta 1}[(Li_{3/21+\delta 1}Ni_{4/21-\delta 1})_{\alpha}(Mn_{12/21}Ni_{2/21})_{\beta}]O_2$ composition (with $\delta_1 = 0.06$ and $Li/Ni = \frac{1}{2}$) and rest of Mn^{4+} are in Ni,Mn-environment such as $Li_{1-\delta 2}Ni_{\delta 2}[Ni_{1-y}Mn_y]O_2$ ($y < \frac{1}{2}$). For $LiNi_{0.5}Mn_{0.5}O_2$ with $\delta = 0.099$, the local environment is as follow: 49% of Mn^{4+} will have 2.57 Mn^{4+}, 1.63 Ni^{2+} and 1.80 Li^{+} ions, while 51% of Mn^{4+} will be surrounded by 3.42 Ni^{2+} and 2.58 Mn^{4+} ions. The average Mn^{4+}-environment will include 2.52 Mn, 2.59 Ni and 0.89 Li. As was at Li/Ni-series, the Ni ions residing the Li-sites are also included in the calculation of local Ni to Mn-ratio. For the sake of comparison, the composition of the first coordination sphere of Mn^{4+} in $LiNi_{0.5}Mn_{0.5}O_2$ has been determined by Breger et al. using joint NMR and PDF analysis [14]: 2.36 Mn, 3.11 Ni, 0.53 Li. As one can see, there is a satisfactory agreement. The

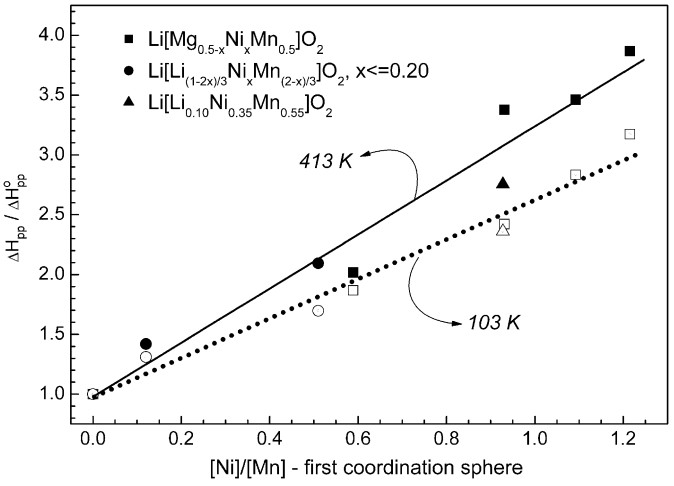

Fig. 11. The normalized EPR line width, $\Delta H_{pp}/\Delta H^{o}_{pp}$, on the local [Ni]/[Mn]-ratio (first coordination sphere) for of $Li[Li_{(1-2x)/3}Ni_xMn_{(2-x)/3}]O_2$ ($0 \leqslant x \leqslant 0.20$, ΔH^{o}_{pp} of Mn^{4+} in $Li[Li_{1/3}Mn_{2/3}]O_2$), $LiMg_{0.5-x}Ni_xMn_{0.5}O_2$ ($0 \leqslant x \leqslant 0.50$, ΔH^{o}_{pp} of Mn^{4+} in $Li[Mg_{0.5}Mn_{0.5}]O_2$) and $Li[Li_{0.10}Ni_{0.35}Mn_{0.55}]O_2$ (ΔH^{o}_{pp} of Mn^{4+} in $Li[Mg_{0.5}Mn_{0.5}]O_2$). The line width is determined at 103 and 413 K.

same is related to Ni-environment. Concerning Ni ions, the model predicts three types of Ni-environment: 29% of Ni will have 5.1Mn and 0.9Ni neighbours (α-site); 20% of Ni — 2.57Mn, 1.63Ni and 1.80Li (β-site) and 51% of Ni — $3.52Ni^{2+}$ and $2.48Mn^{4+}$ ions. In addition, some of Ni ions occupy the Li-sites due to the cationic mixing. From the EPR experiments both at low and high frequency, it appears that all Ni ions are turn off and remains unobservable by EPR. The average environment of Ni in the transition metal layers only will be: 3.30Mn, 2.33Ni and 0.37Li. This is in agreement with the Ni-environment determined by Bréger et al. [14]: 3.64Mn, 1.70Ni and 0.64Li.

To check the validity of the proposed model, Fig. 11 gives the experimentally derived dependence of the normalized EPR line width, $\Delta H_{pp}/\Delta H^{o}_{pp}$, for $LiMg_xNi_{0.5-x}Mn_{0.5}O_2$ and $Li[Li_{(1-2x)/3}Ni_xMn_{(2-x)/3}]O_2$, on the local [Ni]/[Mn]-ratio in the first metal shell of the Mn^{4+} ions. As one can expect, the experimentally obtained results display a linear dependence at lower and higher registration temperature (103 and 413 K, respectively). This supports the proposed model for local cationic distribution in $LiMg_{0.5-x}Ni_xMn_{0.5}O_2$.

4. Conclusions

It was shown that for $LiMg_{0.5-x}Ni_xMn_{0.5}O_2$ and $Li[Li_{(1-2x)/3}Ni_xMn_{(2-x)/3}]O_2$ an EPR response from Mn^{4+} ions is detected only, while the Ni^{2+} ions remain EPR silent even at the higher frequency used. For diamagnetically diluted oxides, $LiMg_{0.25}Ni_{0.25}Mn_{0.5}O_2$ and $Li[Li_{0.10}Ni_{0.35}Mn_{0.55}]O_2$, two types of Mn^{4+} ions characterized with different cationic environment, are detected by high-field experiments. In the X-band, comparative analysis of the EPR line width of Mn^{4+} ions in $LiMg_{0.5-x}Ni_xMn_{0.5}O_2$ compositions shows that a fraction of Mn^{4+} are in the environment resembling the ordered "α,β"-type arrangement in $Li_{1-\delta1}Ni_{\delta1}[Li_{(1-2x)/3+\delta1}Ni_{2x/3-\delta1})_\alpha(Mn_{(2-x)/3}Ni_{x/3})_\beta]O_2$ (where $x=\frac{2}{7}$ and $\delta_1=0.06$ were calculated), while the rest of Mn^{4+} are in the Ni, Mn-environment corresponding to the $Li_{1-\delta2}Ni_{\delta2}[Ni_{1-y}Mn_y]O_2$ ($y<\frac{1}{2}$) composition with a statistical Ni,Mn distribution. This study demonstrates the applicability of EPR spectroscopy to the structural characterization of local cationic distributions in oxides containing more than one paramagnetic species.

Acknowledgments

Authors are indebted to the National Science Fund of Bulgaria (Contract no. Ch1304/2003) for financial support. R.S. is grateful to the EC for a grant within "Access to Research Infrastructure action of the Improving Human Potential Programme"-European Community having enabled her to perform the high-frequency EPR measurements at a High Magnetic Field Laboratory in Grenoble, France. The authors are very grateful to Dr. Anne-Laure Barra (High Magnetic Field Laboratory in Grenoble, France) for her help.

References

[1] M.E. Spahr, P. Novák, B. Schnyder, O. Haas, R. Nesper, J. Electrochem. Soc. 145 (1998) 1113.
[2] T. Ohzuku, Y. Makimura, Chem. Lett. (2001) 744.
[3] Z. Lu, D.D. MacNeil, J.R. Dahn, Electrochem. Solid-State Lett. 4 (2001) A191.
[4] J.-S. Kim, G.S. Johnson, M.M. Thackeray, Electrochem. Commun. 4 (2002) 205.
[5] L. Zhang, H. Noguchi, M. Yoshio, J. Power Sources 110 (2002) 57.
[6] M.S. Whittingham, Chem. Rev. 104 (2004) 4271.
[7] Z. Lu, L.Y. Beaulieu, R.A. Donaberger, C.L. Thomas, J.R. Dahn, J. Electrochem. Soc. 149 (2002) A778.
[8] Z. Lu, Z. Chen, J.R. Dahn, Chem. Mater. 15 (2003) 3214.
[9] J.-S. Kim, C.S. Johnson, J.T. Vaughey, M.M. Thackeray, S.A. Hackney, W. Yoon, C.P. Grey, Chem. Mater. 16 (2004) 1996.
[10] W.-S. Yoon, S. Iannopollo, C.P. Grey, D. Carlier, J. Gorman, J. Reed, G. Ceder, Electrochem. Solid-State Lett. 7 (2004) A167.
[11] M. Saiful Islam, R. Andrew Davis, J.D. Gale, Chem. Mater. 15 (2003) 4280.
[12] Y.S. Meng, G. Ceder, C.P. Grey, W.-S. Yoon, Y. Shao-Horn, Electrochem. Solid-State Lett. 7 (2004) A155.
[13] V. der Ven, G. Ceder, Electrochem. Commun. 6 (2004) 1045.
[14] J. Bréger, N. Dupré, P. Chupas, P.L. Lee, T. Proffen, J. Parise, C.P. Grey, J. Am. Chem. Soc. 127 (2005) 7529.
[15] W.-S. Yoon, C.P. Grey, M. Balasubramanian, X.-Q. Yang, J. McBreen, Chem. Mater. 15 (2003) 3161.
[16] S.-H. Kang, J. Kim, M.E. Stoll, D. Abraham, Y.K. Sun, K. Amine, J. Power Sources 112 (2002) 41.
[17] J. Krzystek, J.-H. Park, M.W. Meisel, M.A. Hitchman, H. Stratemeier, L.-C. Brunel, J. Tesler, Inorg. Chem. 41 (2002) 4478.
[18] E. Zhecheva, R. Stoyanova, Solid State Commun. 135 (2005) 405.
[19] R. Stoyanova, E. Zhecheva, C. Friebel, Solid State Ion. 73 (1994) 1.
[20] C.B. Azzoni, A. Paleari, V. Massarotti, M. Bini, D. Capsoni, Phys. Rev. B 53 (1995) 703.
[21] A.-L. Barra, G. Chouteau, A. Stepanov, A. Rougier, C. Delmas, Eur. Phys. J. B 7 (1999) 551.
[22] F. Reynaud, D. Mertz, F. Celestini, J.-M. Debierre, A.M. Ghorayeb, P. Simon, A. Stepanov, J. Voiron, C. Delmas, Phys. Rev. Lett. 86 (2001) 3638.
[23] R. Stoyanova, E. Zhecheva, R. Alcántara, P. Lavela, J.-L. Tirado, Solid State Commun. 102 (1997) 457.
[24] D. Capsoni, M. Bini, G. Chiodelli, V. Massarotti, M.C. Mozatti, A. Comin, Phys. Chem. Chem. Phys. 3 (2001) 2162.
[25] R. Stoyanova, M. Gorova, E. Zhecheva, J. Phys. Chem. Solids 61 (2000) 609.
[26] D. Capsoni, M. Bini, G. Chiodelli, V. Massarotti, M.C. Mozatti, C. Azzoni, Solid State Commun. 125 (2003) 179.
[27] E. Zhecheva, R. Stoyanova, M. Gorova, P. Lavela, J.L. Tirado, Solid State Ion. 140 (2001) 19.
[28] S. Mandal, R.M. Rojas, J.M. Amarilla, P. Calle, N.V. Kosova, V.F. Anufrienko, J.M. Rojo, Chem. Mater. 14 (2002) 1598.
[29] R. Alcántara, M. Jaraba, P. Lavela, J.L. Tirado, E. Zhecheva, R. Stoyanova, Chem. Mater. 16 (2004) 1573.
[30] S.-H. Kang, K. Amine, J. Power Sources 119–121 (2003) 150.
[31] P. Strobel, A. Ibarra-Palos, M. Anne, C. Poinsignon, A. Crisci, Solid State Sci. 5 (2003) 1009.
[32] Z.P. Guo, S. Zhang, G.X. Wang, H.K. Liu, S.X. Dou, J. Alloy. Compd. 348 (2003) 231.
[33] R. Prassard, R. Benedek, M.M. Thackeray, Phys. Rev. B 71 (2005) art. No. 134111.
[34] J. Rodríguez-Carvajal, in: Proceedings of the Satellite Meeting on Powder Diffraction of the XV Congress of the IUCr, 1990, p. 127.
[35] J.H. Van Vleck, Phys. Rev. 74 (1948) 1168.

[36] P.W. Anderson, P.W. Weiss, Rev. Mod. Phys. 25 (1953) 269.
[37] T. Morya, Prog. Theor. Phys. Kyoto 16 (1956) 23.
[38] P. Tarte, A. Rulmont, C.R. Liégeois-Duyckaerts, J.M. Winand, Solid State Ion. 42 (1990) 177.
[39] E. Zhecheva, R. Stoyanova, Solid State Ion. 66 (1993) 143.
[40] V. Massarotti, D. Capsoni, M. Bini, C.B. Azzoni, J. Solid State Chem. 128 (1997) 80.
[41] R. Stoyanova, M. Gorova, E. Zhecheva, J. Phys. Chem. Solids 61 (2000) 615.
[42] W. Branford, M.A. Green, D.A. Neumann, Chem. Mater. 14 (2002) 1649.
[43] C. Masquelier, M. Tabuchi, K. Ado, R. Kanno, Y. Kobayashi, Y. Maki, O. Nakamura, J.B. Goodenough, J. Solid State Chem. 123 (1996) 255.
[44] J.E. Greedan, N.P. Raju, A.S. Wills, C. Morin, S.M. Shaw, J.N. Reimers, Chem. Mater. 10 (1998) 3058.
[45] K.K. Anderson, A.L. Barra, Spectrochim. Acta A 58 (2002) 1101.
[46] P. Strobel, B. Lambert-Anderson, J. Solid State Chem. 75 (1988) 90.